Published in final edited form as:
ACS Nano. 2013 November 26; 7(11): 9675–9683. doi:10.1021/nn404079v.

In Vitro Selection of Shape-Changing DNA Nanostructures Capable of Binding-Induced Cargo Release

Seung Soo Oh[†], **Kory Plakos**[†,‡], **Yi Xiao**[†,‡], **Michael Eisenstein**[†,‡], and **Hyongsok Tom Soh**[†,‡,*]

[†]Materials Department, University of California, Santa Barbara, CA 93106

[‡]Department of Mechanical Engineering, University of California, Santa Barbara, CA 93106

Abstract

Many biological systems employ allosteric regulatory mechanisms, which offer a powerful means of directly linking a specific binding event to a wide spectrum of molecular functionalities. There is considerable interest in generating synthetic allosteric regulators that can perform useful molecular functions for applications in diagnostics, imaging and targeted therapies, but generating such molecules through either rational design or directed evolution has proven exceptionally challenging. To address this need, we present an *in vitro* selection strategy for generating conformation-switching DNA nanostructures that selectively release a small-molecule payload in response to binding of a specific trigger molecule. As an exemplar, we have generated a DNA nanostructure that hybridizes with a separate 'cargo strand' containing an abasic site. This abasic site stably sequesters a fluorescent cargo molecule in an inactive state until the DNA nanostructure encounters an ATP trigger molecule. This ATP trigger causes the nanostructure to release the cargo strand, thereby liberating the fluorescent payload and generating a detectable fluorescent readout. Our DNA nanostructure is highly sensitive, with an EC_{50} of 30 μM, and highly specific, releasing its payload in response to ATP but not to other chemically similar nucleotide triphosphates. We believe that this selection approach could be generalized to generate synthetic nanostructures capable of selective and controlled release of other small-molecule cargos in response to a variety of triggers, for both research and clinical applications.

Keywords

Allostery; Microfluidics; *In vitro* selection; Functional aptamer; ATP; ATMND; Structure-switching

Allostery offers a powerful mechanism for modulating biomolecular functions by linking a specific molecular recognition event to a wide range of downstream functions.[1,2] There are many examples of allostery in nature, wherein the binding of regulatory factors induces dramatic changes in the ligand-binding affinity or catalytic rate of a protein.[3] For example, when adenosine triphosphate (ATP) levels become elevated within a cell, excess ATP binds to the catabolic enzyme phosphofructokinase, reducing its affinity for ligand fructose-6-phosphate, thereby inactivating this pathway until ATP concentrations normalize.[4-6] Nucleic acids also play an important role in the allosteric regulation of gene expression.[7-11] For

*Corresponding author: tsoh@engr.ucsb.edu.

Supporting Information **Available:** Characterization details for SSA molecules, DNA sequence information, experimental condition details. This material is available free of charge *via* the Internet at http://pubs.acs.org.

example, riboswitches have been shown to play critical functions in the biosynthesis and transport of metabolites such as amino acids, nucleotides and vitamins.[12-15]

There is considerable interest in using *in vitro* selection to engineer allosterically-regulated functional nucleic acid aptamers, as these nanostructures could be valuable tools for molecular diagnostics, imaging and targeted therapies.[16-19] Generation of such molecules typically entails the modification of existing aptamers in order to incorporate the new function.[20-23] However, such sequence alterations usually undermine the affinity and specificity of the molecule, and a strategy for directly selecting for the desired function may therefore prove more advantageous. Toward this end, pioneering work from the Ellington,[24,25] Breaker,[26,27] and Famulok groups[28,29] has demonstrated the selection of allosteric ribozymes that exhibit enhanced catalytic activity in response to binding of various ligands. Moreover, there have been several successes in isolating allosterically-regulated aptamers that can fluorescently report binding events.[30-33] Given these precedents, it should be theoretically possible to directly select for molecules capable of many different downstream molecular functions triggered by specific molecular recognition, such as catalysis of synthetic reactions or targeted drug release. However, published examples to date have generally been limited to a handful of applications, most notably binding-induced catalysis with nucleic acid-based templates or fluorescence signaling based on molecular beacons.[24-36] As such, there is an unmet need for versatile selection strategies that can facilitate the generation of molecules capable of performing a broader range of molecular functionalities in response to ligand binding.

To this end, we present a strategy that combines elements of rational design and *in vitro* selection in order to generate structure-switching aptamers (SSAs) capable of controlled cargo release in response to allosteric binding of a specific target molecule. As a model, we generated an SSA that selectively releases a fluorescent cargo (5,6,7-trimethyl-1,8-naphthyridin-2-ylamine; ATMND) in response to heterotropic allosteric binding of its ligand (ATP) through a conformational change (Figure 1A). Our selection technique generated an SSA molecule that exhibits a half-maximal effective concentration (EC_{50}) of ~30 μM, approximately 18-fold more sensitive than a previously reported ATP-responsive signaling aptamer.[37] Furthermore, we demonstrate that our SSA is highly ATP-specific, and does not respond to closely-related chemical analogs. Based on these results, we conclude that it should be feasible to adapt our selection process to generate synthetic nanostructures capable of performing other functionalities for diagnostic and therapeutic applications.

RESULTS AND DISCUSSION

We *in vitro* selected our SSAs from a starting library of DNA molecules, each containing three functional domains (Figure 1B). The central domain (black, 26 bases) hybridizes with a cargo strand (green, 12 bases) that contains an abasic site. This central domain features two flexible linkers composed of four thymidines flanking a guanine-rich motif[38,39] that can fold into a G-quadruplex structure. Such structures exhibit modest affinity for ATP[40] and could potentially promote SSA interaction with ATP, and G-quadruplex folding could subsequently facilitate cargo strand release by reducing the activation energy required for ATP-induced conformational rearrangement. We loaded the ATMND cargo into the abasic site *via* hydrogen bonding with a cytosine in the central domain.[41] ATMND remains stable with quenched fluorescence within the duplex because the ATMND/cytosine pair is further stacked with neighboring GC pairs.[42,43] We flanked the central domain with two randomized recognition domains (cyan, 17 bases each) that were *in vitro* selected to undergo a large conformational change in specific response to ATP binding. Finally, we incorporated primer-binding sites at either end (purple, 20 bases) to enable polymerase chain reaction (PCR) amplification. All sequences are provided in the supporting information (Table S1).

We selected SSA molecules capable of structure-switching by immobilizing the library onto cargo strand-conjugated magnetic beads, and isolating molecules that selectively release from the beads when challenged with ATP (Figure 1C; see Methods for details). Specifically, we prepared ~100 picomoles of our randomized SSA library (see Methods for details) by hybridization with biotinylated cargo strands, allowing the library to be immobilized onto streptavidin (SA)-coated magnetic beads. We blocked the primer-binding sites with complementary DNA to limit their involvement in SSA folding. Next, we challenged the library with ATP and collected molecules that were released from the beads as a result of the cargo strand uncoupling from the central domain in response to ATP-induced structure-switching. We isolated these SSAs using the micromagnetic separation chip (MMS) previously described by our group, which allows highly efficient trapping of beads from a continuous stream.[44,45] After separation, we PCR amplified the enriched SSA pool and generated single-stranded products for the next round of selection.

We performed ten rounds of selection (R1–10; Table S2), systematically applying higher stringency by decreasing the ATP concentration from 1 mM in R1 to 20 μM in R10 (see Methods). To increase specificity, we also performed negative selection from R3 onward using 1 μM SA and 1 μM bovine serum albumin (BSA). We chose these proteins because SA was used for SSA immobilization, while BSA is the most abundant serum protein and therefore the most likely non-target molecule to be encountered in an *in vivo* setting. Importantly, we also performed further negative selection in R7 through R10 with 1 mM guanosine triphosphate (GTP), which has a similar chemical structure to ATP.

After 10 rounds of selection, the enriched pool exhibited clear structure-switching functionality. This was evident when we immobilized the R10 pool on SA-coated magnetic beads and measured the amount of eluent after challenging with ATP at concentrations ranging from 2–100 μM (see Methods). We PCR-amplified and quantitated each eluent *via* gel electrophoresis, and measurement of band intensities revealed that the amount of eluted SSA increased in parallel with ATP concentration (Figure 2A). We determined that the amount of SSAs eluted by 100 μM ATP was 9-fold greater than the quantity of unbound SSAs observed in the absence of ATP. It should be noted that even in the absence of a trigger molecule, these molecules exist in a state of equilibrium in which a small fraction of SSAs will be unbound from their cargo strand (Figure 2A, 0 μM ATP lane). These data suggest that ATP indeed triggered SSA structure-switching, resulting in de-hybridization between the cargo strand and the central domain. In order to quantify the concentration of ATP required to trigger structure-switching, we measured the EC_{50} of the R10 pool.[46] Assuming Langmuirian binding between SSA and ATP, we obtained the EC_{50} value by fitting a curve to the band intensities using the equation $Y = B + (M - B) \times X/(EC_{50} + X)$, where Y is the band intensity, X is the ATP concentration, and B and M are the baseline and maximum band intensities, respectively. Based on these calculations, we found that the EC_{50} of the R10 pool was 22.1 ± 3.5 μM (Figure 2B).

We obtained 45 SSA sequences from the R10 pool after cloning into *E. coli*, and found that the pool contained two dominant consensus sequences (SSA-1 and SSA-2), which constituted 96% of the clones analyzed (Table 1). Interestingly, SSA-2 contains a single T→C mutation within the fixed sequence of the central domain at the 18th base from the 3′ end (labeled red in Table 1); based on previous reports, this may facilitate cargo strand release by weakening duplex formation.[31] We next used quantitative real-time PCR (RT-PCR)[47] to characterize SSA structure-switching function by measuring the quantity of each SSA eluted from magnetic beads following displacement of the cargo strand upon ATP binding. Since the PCR primer-binding sites on the SSA library molecules were blocked by complementary sequences during selection, we assume they play no meaningful role in aptamer folding or binding; as such, these sequences were eliminated from SSA-1 and -2 for

this and subsequent experiments. We found that the fraction of SSAs that undergo structure-switching rapidly saturates to its maximum value even at relatively low target concentrations. For example, at 100 μM ATP, the cargo strand was displaced from 82.6% of SSA-1 and 77.4% of SSA-2 molecules. By titrating ATP, we measured EC_{50} = 37.6 ± 8.8 μM for SSA-1 and 33.7 ± 7.8 μM for SSA-2 (Figure 3A, B). Both molecules exhibited higher sensitivity than previously-described structure-switching signaling aptamers triggered by ATP, with 18-fold better EC_{50}.[37] Importantly, our two SSA molecules are highly ATP-specific and do not respond even to close chemical analogs. We found that binding to GTP was substantially lower than to ATP for both SSA-1 (Figure 3A) and SSA-2 (Figure 3B). Interestingly, both SSAs also showed negligible binding to cytosine triphosphate (CTP), which was not used in negative selection (Figure 3A, B). Based on this result, we postulate that the SSA recognition site on ATP is unlikely to be the phosphate group.

We next showed that SSA-1 effectively releases ATMND cargo upon binding ATP. We loaded ATMND into the abasic site of the cargo strand (see Methods), such that its fluorescence was effectively quenched by pseudo-base pairing with cytosine within the central domain (Figure 3C, black trace and Figure S1). The quantity of ATMND released into solution increased greatly upon addition of ATP (Figure 3C). We measured an EC_{50} of 29.9 ± 5.8 μM resulting from ATMND release, measured at its fluorescence peak of 405 nm (Figure S2). We note that this is in close agreement with the EC_{50} value obtained *via* RT-PCR (Figure 3A), adding further evidence that the structure-switching mechanism is responsible for ATMND release and that this release occurs efficiently in response to ATP. As a negative control, we confirmed that the initial library shows minimal ATMND release even in response to 1 mM ATP (Figure 3C, purple trace). Cargo release by SSA-1 proved highly ATP-specific, with minimal ATMND release in response to 1 mM GTP or CTP (Figure 3D, blue and green traces). Interestingly, SSA-2 showed significantly lower ATMND release compared to SSA-1 in the same ATP concentration range (Figure S3). We also observed no difference of behavior between the SSA-2 with and without the T-to-C mutation (red in Table 1), inferring that this point mutation is not the main cause of the difference in affinity between SSA-1 and SSA-2. The basis for this difference is currently under investigation, but we suspect that SSA-2 does not function properly in free solution and requires a solid support. In keeping with this hypothesis, we observed that the central domain of SSA-2 is flanked by TCGGCT and TCCGGCT motifs (where the second motif contains the relevant T-to-C mutation), which are highly similar to a binding motif found in many streptavidin aptamers.[48-50] Accordingly, we found that SSA-2 indeed exhibits higher affinity to streptavidin than SSA-1, as evidenced by a ~20-fold increase in binding to streptavidin-coated beads for SSA-2 relative to SSA-1 at 100 nM concentration (Figure S4). From these observations, we infer that interaction between SSA-2 and the streptavidin-coated beads used for immobilization may contribute to the observed solid support dependence.

Finally, we investigated the structure of SSA-1 after it releases the cargo strand upon binding to ATP (Figure 4A). We found that the SSA-1 structure can be categorized into four main domains: a short stem (green), an ATP-binding motif (blue), an incompatibly-paired linker region (black) and the pre-designed G-quadruplex sequence (red). Interestingly, the ATP-binding motif contains CTGGGGGAG and CGGAGGA sequences (blue), similar to motifs observed in previously-reported ATP aptamers,[51] and these presumably form a pocket that recognizes ATP. We suspect that the stem region (green) may play an important role in ATP-induced shape-changing. The hybridization energy for this region is weaker than that of the relatively stable cargo strand-central domain duplex, and as such this stem will form as long as the duplex structure of SSA-1 is fully intact. However, if ATP binding disrupts the interaction between the cargo strand and the central domain, stem formation becomes energetically favorable and subsequently promotes the conformational change of

SSA-1. To further confirm that such a change in the SSA structure is responsible for the release of ATMND upon ATP binding, we modified SSA-1 with 6-carboxyfluorescein (FAM) at its 5′ end and with Black Hole Quencher (BHQ1) at its 3′ end (Figure 4A), and challenged this construct with increasing concentrations of ATP. We observed a large fluorescence decrease for SSA-1 at increasing ATP concentrations, indicating that the structure indeed undergoes a conformational change and reduces the effective distance between the fluorophore and quencher. (Figure 4B). When challenged with 1 mM ATP, SSA-1 yielded ~80% lower fluorescence intensity than in the absence of ATP. We measured an EC_{50} of 31.8 ± 4.8 μM based on the ATP-dependent decrease in fluorescence intensity (Figure 4C), similar to the EC_{50} values measured above.

CONCLUSION

In this work, we have shown that the combination of a rationally designed scaffold with a stringent, *in vitro* selection strategy offers an effective means for generating allosterically-regulated, shape-changing DNA nanostructures. The SSA molecules that we generated bind specifically to ATP—but not other nucleotide triphosphates—and subsequently undergo a large conformational change, which results in selective release of a sequestered ATMND cargo molecule. Beyond their excellent specificity, our SSAs also display high sensitivity: SSA-1 was activated by ATP with an EC_{50} of ~30 μM, which is ~18-fold lower than previous reported ATP-responsive DNA constructs.[37] Furthermore, we determined that the EC_{50} of SSA-1 can be modulated by varying the cargo strand concentration, with an increase in the concentration of cargo strand yielding an increased EC_{50} (Figure S5). For example, a 1:30 ratio of SSA-1:cargo strand at 30 nM yielded an EC_{50} of 92.0 ± 31.7 μM, 3-fold greater than when these molecules were present in a 1:1.5 ratio at the same total concentration. This indicates that SSA sensitivity can be fine-tuned as desired for specific applications.

We have identified a number of other opportunities to further improve the performance of our SSAs. For example, we observed that background dissociation of the cargo strand in the absence of ATP binding (see Figure 2A) causes a notable reduction in SSA enrichment during the selection process. We envision that systematic application of stronger hybridization pressure through alternative cargo strand design or performing selection rounds at lower temperatures may further improve the selection efficiency. Moreover, we found that our machine-synthesized library was vulnerable to a biased distribution of bases, which subsequently affected library diversity (see Methods for details). Despite this, we were able to discover SSAs with excellent affinity and specificity and the use of higher diversity library in the future may lead to molecules with better performance.

We employed ATMND as a cargo for proof of concept, because its fluorescent readout offers a convenient means for quantifying efficiency of release. However, we envision that other hydrophilic, small-molecule payloads could likewise be embedded in a similar nanostructure. This selection strategy could thus potentially facilitate the synthesis of a diverse array of molecules for specialized controlled-release applications, including constructs that stably retain their therapeutic payload in an inactive state until they encounter a biomarker indicative of a particular disease state or infectious agent. In this fashion, creative selection strategies that can link a molecular recognition event directly to a useful molecular function could open interesting new avenues in the realm of molecular diagnostics or targeted therapies.

METHODS

Reagents

The DNA library, cargo strand, biotinylated cargo strand, primer site-blocking strands, forward primer, biotinylated reverse primer, and unmodified reverse primer sequence (see Supporting Information, Table S1) were synthesized and purified by Integrated DNA Technologies (Coralville, IA). Each single-stranded DNA (ssDNA) library component consists of a central 60-mer region flanked by two 20-mer PCR primer sequences. The central region includes a 26-base cargo strand-binding sequence flanked by two 17-base randomized sequences. HotStarTaq Master Mix was purchased from Qiagen (Hilden, Germany). MyOne Streptavidin C1 Dynabeads were purchased from Life Technologies (Carlsbad, CA). ATP was purchased from LKT Laboratories (St. Paul, MN), and GTP, CTP, SA and BSA were purchased from Sigma-Aldrich (St. Louis, MO) and used without further purification. ATMND was purchased from Enamine (Kiev, Ukraine). The iQ SYBR Green Supermix was purchased from Bio-Rad Laboratories (Hercules, CA) for RT-PCR experiments.

SSA Library Preparation and Immobilization on Magnetic Beads

A random ssDNA library was synthesized with machine-mixed bases as a 100 μM solution, and its concentration was confirmed *via* UV-vis measurement. We began with 100 pmol of ssDNA library synthesized from machine-mixed nucleotides (1 μL of the 100 μM stock). To characterize diversity, we picked and sequenced 50 random clones from the machine-synthesized library. These were all unique (Table S3), but we also identified a synthetic bias favoring A and G incorporation, with a distribution of 30.4%, 20.1%, 20.2% and 29.3% for A, T, C and G, respectively. The library was mixed with 150 pmol of each primer site-blocking strand and 150 pmol of biotinylated cargo strand, and hybridized in 20 μL 1× Perfect Match buffer (PM; 1 mM sodium phosphate, 1 mM NaCl and 30 mM $MgCl_2$, pH 6.8) by heating at 95 °C for 10 min and slowly cooling down to room temperature (RT) over 3 hrs. The prepared SSA library mixture was incubated overnight at RT with 300 μL of SA-coated magnetic beads in 150 mM phosphate buffer (1 M NaCl, 5mM $MgCl_2$, and 0.01% Tween-20 (v/v), pH 7.5). Nonspecifically bound DNA molecules were removed by washing library-bead assemblies with buffer in which NaCl concentration was gradually decreased from 1 M to 1 mM. The beads were then resuspended in 300 μL of 1× ATP binding buffer (ATPBB; 20 mM Tris, 300 mM NaCl, and 5 mM $MgCl_2$, pH 7.4) and incubated at RT overnight to maximize the amount of cargo strand-immobilized duplex SSA library molecules on the beads and minimize the amount of non-specifically released SSAs prior to selection, increasing the likelihood that SSA candidates present in solution have been liberated in an ATP-dependent fashion.

In vitro SSA Selection

In R1, the library-bead assemblies were challenged with 1 mM ATP in 300 μL of 1× ATPBB for 2 hrs at RT. SSA molecules that underwent ATP-induced structure-switching were separated from library-bound beads in two steps. First, the bead waste was separated in a conventional tube with a magnetic particle concentrator (Life Technologies). The collected supernatant was then further purified in an MMS chip to achieve exceptional purity of the desired SSA molecules, followed by PCR amplification and ssDNA generation. The resulting ssDNA pool was used as a library for the next round. Over ten rounds of selection, we systematically decreased the ATP concentration to apply higher selection stringency (see Table S2). From R3 on, we also performed negative selections using 1 μM BSA and 1 μM SA, and added 1 mM GTP from R7–10 as negative selection before positive selection against ATP. The negative selections were performed in 300 μL of 1× ATPBB for 2 hrs at RT.

PCR Amplification

100 μL PCR reactions contained 50 μL HotStarTaq Master Mix, 0.25 μL 100 μM forward and biotinylated reverse primer, 10 μL collected SSA molecules, and 39.5 μL nuclease-free water. HotStarTaq polymerase was activated prior to PCR by heating reactions to 95 °C for 15 min, followed by 25 cycles of a three-step PCR (30-s denaturation at 95 °C, 30-s annealing at 56 °C, 30-s extension at 72 °C). 8 μL of PCR mixture were collected and resolved on 10% PAGE-TBE (1× TBE: 89 mM Tris-borate, 2 mM Na_2EDTA, pH 8.3) gel to determine the optimal PCR amplification cycle number with minimal byproducts. Collected SSA pools from each round were PCR amplified at the optimized cycle number.

ssDNA Generation

After full PCR amplification, biotinylated, double-stranded DNA (dsDNA) was purified using the MiniElute PCR Purification Kit (Qiagen), and purified dsDNA was incubated with 150 μL of Dynabeads MyOne Streptavidin C1 for 2 hrs at RT. ssDNAs were eluted from the dsDNA-bead assemblies *via* addition of 100 mM NaOH. After 4-min incubation at RT, the supernatant was collected and neutralized with 1N HCl, followed by desalting of collected ssDNAs. The resulting ssDNA pool was quantified *via* UV-visible measurement at 260 nm.

Cloning and Sequencing of Isolated SSAs

After 10 rounds of selection, the selected SSA pool was PCR-amplified with unmodified forward and reverse primers at an optimized PCR cycle number determined by pilot PCR. These PCR products were then purified by the MiniElute PCR Purification Kit (Qiagen) and cloned into *E. coli* using the TOPO TA cloning kit (Life Technologies). Colonies were randomly picked and sequenced at the GENEWIZ San Diego Laboratory. The sequences were analyzed and aligned using Geneious v5.1 (Biomatters; New Zealand).

Structure-switching characterization using quantitative PCR (qPCR)

5 pmol of individual SSA ssDNA sequences prepared as described above were immobilized on ~2×10^8 SA magnetic beads. Our qPCR measurement confirmed that 60% of our SSAs were immobilized after the preparation step. The SSA/bead assemblies were challenged with ATP at varying concentrations from 2–100 μM in 100 μL of 1× ATPBB for 2 hrs at RT. The quantities of SSAs released as a result of binding-induced structure-switching were subsequently determined by qPCR. Each PCR reaction contained 10 μL iQ SYBR Green Supermix, 8.8 μL PCR water, 0.1 μL each of 0.1 mM forward and reverse primers and 1 μL DNA template. The fluorescence signals of the prepared samples were monitored using the iQ 5 multi-color qPCR Detection System (Bio-Rad), and a C_T value was subsequently determined for each ATP concentration. A qPCR standard curve was also obtained to show that C_T values are linearly related to the initial number of SSA molecules over four orders of magnitude (Figure S6). All samples were tested in triplicate, and the PCR efficiencies were calculated from the linear regression slopes through each set of data, using the equation $E = (10^{-1/m} - 1)$, where E is PCR efficiency and m is the slope of the linear regression (Figure S6). Based on the standard curve, the C_T values were extrapolated to the quantities of SSA molecules and the EC_{50} was calculated from the calibrated curve fitting using the equation $Y = B + (M - B) \times X/(EC_{50} + X)$ where X is the ATP concentration, and B and M are the baseline and saturation quantity of released SSA molecules, respectively.

SSA Characterization using Fluorescence Measurements

We prepared 5 μM SSA or random library DNA, which we then hybridized with a cargo sequence with an abasic site (7.5 μM) in 50 μL 1× ATPBB, along with 0.5 μL of 50 μM ATMND. Mixtures were transferred to a black 96-well microplate (Microfluor 2, Thermo Scientific; Waltham, MA), and challenged by varying concentrations of ATP ranging from

1–1000 μM for 2 hrs at 4 °C. Each fluorescent emission profile was monitored in a 370–700 nm wavelength range using a Tecan microplate reader (San Jose, CA) with the follow settings: excitation wavelength= 358 nm, excitation bandwidth= 5 nm, and emission bandwidth= 5 nm. This allowed us to determine the largest emission peak for each trigger concentration.

Supplementary Material

Refer to Web version on PubMed Central for supplementary material.

Acknowledgments

We are grateful for financial support from the National Institutes of Health (R01A1085583, U54 DK093467), the Department of Defense (W81XWH-09-0698) and the Institute of Collaborative Biotechnologies through the Army Research Office (W911NF-09-0001 and W911NF-10-2-0114). Microfabrication was carried out in the Nanofabrication Facility at UCSB.

REFERENCES

1. Goodey NM, Benkovic SJ. Allosteric Regulation and Catalysis Emerge *via* a Common Route. Nature Chem. Biol. 2008; 4:474–482. [PubMed: 18641628]
2. Smock RG, Gierasch LM. Sending Signals Dynamically. Science. 2009; 324:198–203. [PubMed: 19359576]
3. Huang ZM, Zhu LA, Cao Y, Wu G, Liu XY, Chen YY, Wang Q, Shi T, Zhao YX, Wang YF, et al. ASD: a Comprehensive Database of Allosteric Proteins and Modulators. Nucleic Acids Res. 2011; 39:D663–D669. [PubMed: 21051350]
4. Uyeda K, Racker E. Regulatory Mechanisms in Carbohydrate Metabolism. 7. Hexokinase and Phosphofructokinase. J. Biol. Chem. 1965; 240:4682–4688. [PubMed: 4221248]
5. Paetkau V, Lardy HA. Phosphofructokinase - Correlation of Physical and Enzymatic Properties. J. Biol. Chem. 1967; 242:2035–2042. [PubMed: 4225717]
6. Kemp RG, Krebs EG. Binding of Metabolites by Phosphofructokinase. Biochemistry. 1967; 6:423–434. [PubMed: 4227735]
7. Mandal M, Breaker RR. Gene Regulation by Riboswitches. Nat. Rev. Mol. Cell Biol. 2004; 5:451–463. [PubMed: 15173824]
8. Djuranovic S, Zinchenko MK, Hur JK, Nahvi A, Brunelle JL, Rogers EJ, Green R. Allosteric Regulation of Argonaute Proteins by miRNAs. Nat. Struct. Mol. Biol. 2010; 17:144–150. [PubMed: 20062058]
9. Chaires JB. Allostery: DNA Does It, Too. ACS Chem. Biol. 2008; 3:207–209. [PubMed: 18422302]
10. Chenoweth DM, Dervan PB. Allosteric Modulation of DNA by Small Molecules. Proc. Natl. Acad. Sci. U. S. A. 2009; 106:13175–13179. [PubMed: 19666554]
11. Kim S, Brostromer E, Xing D, Jin JS, Chong SS, Ge H, Wang SY, Gu C, Yang LJ, Gao YQ, et al. Probing Allostery through DNA. Science. 2013; 339:816–819. [PubMed: 23413354]
12. Nahvi A, Sudarsan N, Ebert MS, Zou X, Brown KL, Breaker RR. Genetic Control by a Metabolite Binding mRNA. Chem. Biol. 2002; 9:1043–1049. [PubMed: 12323379]
13. Winkler W, Nahvi A, Breaker RR. Thiamine Derivatives Bind Messenger RNAs Directly to Regulate Bacterial Gene Expression. Nature. 2002; 419:952–956. [PubMed: 12410317]
14. Mandal M, Lee M, Barrick JE, Weinberg Z, Emilsson GM, Ruzzo WL, Breaker RR. A Glycine-Dependent Riboswitch that Uses Cooperative Binding to Control Gene Expression. Science. 2004; 306:275–279. [PubMed: 15472076]
15. Mandal M, Boese B, Barrick JE, Winkler WC, Breaker RR. Riboswitches Control Fundamental Biochemical Pathways in Bacillus Subtilis and Other Bacteria. Cell. 2003; 113:577–586. [PubMed: 12787499]
16. Famulok M, Hartig JS, Mayer G. Functional Aptamers and Aptazymes in Biotechnology, Diagnostics, and Therapy. Chem. Rev. 2007; 107:3715–3743. [PubMed: 17715981]

17. Vinkenborg JL, Karnowski N, Famulok M. Aptamers for Allosteric Regulation. Nature Chem. Biol. 2011; 7:519–527. [PubMed: 21769099]
18. Plaxco KW, Soh HT. Switch-Based Biosensors: a New Approach towards Real-Time, *in vivo* Molecular Detection. Trends Biotechnol. 2011; 29:1–5. [PubMed: 21106266]
19. Krishnan Y, Simmel FC. Nucleic Acid Based Molecular Devices. Angew. Chem. Int. Edit. 2011; 50:3124–3156.
20. Tang J, Breaker RR. Rational Design of Allosteric Ribozymes. Chem. Biol. 1997; 4:453–459. [PubMed: 9224568]
21. Silverman SK. Rube Goldberg Goes (Ribo)nuclear? Molecular Switches and Sensors Made from RNA. RNA-Publ. RNA Soc. 2003; 9:377–383.
22. Nutiu R, Li YF. Structure-Switching Signaling Aptamers: Transducing Molecular Recognition into Fluorescence Signaling. Chem.-Eur. J. 2004; 10:1868–1876. [PubMed: 15079825]
23. Liu JW, Cao ZH, Lu Y. Functional Nucleic Acid Sensors. Chem. Rev. 2009; 109:1948–1998. [PubMed: 19301873]
24. Robertson MP, Ellington AD. In Vitro Selection of an Allosteric Ribozyme that Transduces Analytes to Amplicons. Nature Biotechnol. 1999; 17:62–66. [PubMed: 9920271]
25. Robertson MP, Ellington AD. *In Vitro* Selection of Nucleoprotein Enzymes. Nature Biotechnol. 2001; 19:650–655. [PubMed: 11433277]
26. Koizumi M, Soukup GA, Kerr JNQ, Breaker RR. Allosteric Selection of Ribozymes that Respond to the Second Messengers cGMP and cAMP. Nature Struct. Biol. 1999; 6:1062–1071. [PubMed: 10542100]
27. Zivarts M, Liu Y, Breaker RR. Engineered Allosteric Ribozymes that Respond to Specific Divalent Metal Ions. Nucleic Acids Res. 2005; 33:622–631. [PubMed: 15681614]
28. Piganeau N, Jenne A, Thuillier V, Famulok M. An Allosteric Ribozyme Regulated by Doxycyline. Angew. Chem. Int. Edit. 2000; 39:4369–4373.
29. Piganeau N, Thuillier V, Famulok M. *In Vitro* Selection of Allosteric Ribozymes: Theory and Experimental Validation. J. Mol. Biol. 2001; 312:1177–1190. [PubMed: 11580234]
30. Ferguson A, Boomer RM, Kurz M, Keene SC, Diener JL, Keefe AD, Wilson C, Cload ST. A Novel Strategy for Selection of Allosteric Ribozymes Yields RiboReporter (TM) Sensors for Caffeine and Aspartame. Nucleic Acids Res. 2004; 32:1756–1766. [PubMed: 15026535]
31. Nutiu R, Li Y. *In Vitro* Selection of Structure-Switching Signaling Aptamers. Angew. Chem. Int. Edit. 2005; 44:1061–1065.
32. Morse DP. Direct Selection of RNA Beacon Aptamers. Biochem. Biophys. Res. Commun. 2007; 359:94–101. [PubMed: 17533112]
33. Oh SS, Plakos K, Lou X, Xiao Y, Soh HT. *In Vitro* Selection of Structure-Switching, Self-Reporting Aptamers. Proc. Natl. Acad. Sci. U. S. A. 2010; 107:14053–14058. [PubMed: 20660786]
34. Komatsu Y, Nobuoka K, Karino-Abe N, Matsuda A, Ohtsuka E. *In Vitro* Selection of Hairpin Ribozymes Activated with Short Oligonucleotides. Biochemistry. 2002; 41:9090–9098. [PubMed: 12119023]
35. Rajendran M, Ellington AD. *In Vitro* Selection of Molecular Beacons. Nucleic Acids Res. 2003; 31:5700–5713. [PubMed: 14500834]
36. Rajendran M, Ellington AD. Selection of Fluorescent Aptamer Beacons that Light Up in the Presence of Zinc. Anal. Bioanal. Chem. 2008; 390:1067–1075. [PubMed: 18049815]
37. Nutiu R, Li YF. Structure-Switching Signaling Aptamers. J. Am. Chem. Soc. 2003; 125:4771–4778. [PubMed: 12696895]
38. Li YF, Geyer CR, Sen D. Recognition of Anionic Porphyrins by DNA Aptamers. Biochemistry. 1996; 35:6911–6922. [PubMed: 8639643]
39. Travascio P, Li YF, Sen D. DNA-Enhanced Peroxidase Activity of a DNA Aptamer-Hemin Complex. Chem. Biol. 1998; 5:505–517. [PubMed: 9751647]
40. Kong DM, Xu J, Shen HX. Positive Effects of ATP on G-Quadruplex-Hemin DNAzyme-Mediated Reactions. Anal. Chem. 2010; 82:6148–6153. [PubMed: 20552961]

41. Sato Y, Nishizawa S, Yoshimoto K, Seino T, Ichihashi T, Morita K, Teramae N. Influence of Substituent Modifications on the Binding of 2-amino-1,8-naphthyridines to Cytosine opposite an AP Site in DNA Duplexes: Thermodynamic Characterization. Nucleic Acids Res. 2009; 37:1411–1422. [PubMed: 19136458]

42. Xiang Y, Tong AJ, Lu Y. Abasic Site-Containing DNAzyme and Aptamer for Label-Free Fluorescent Detection of Pb2+ and Adenosine with High Sensitivity, Selectivity, and Tunable Dynamic Range. J. Am. Chem. Soc. 2009; 131:15352–15357. [PubMed: 19807110]

43. Sato Y, Nishizawa S, Teramae N. Label-Free Molecular Beacon System Based on DNAs Containing Abasic Sites and Fluorescent Ligands That Bind Abasic Sites. Chem.-Eur. J. 2011; 17:11650–11656. [PubMed: 21953933]

44. Qian JR, Lou XH, Zhang YT, Xiao Y, Soh HT. Generation of Highly Specific Aptamers *via* Micromagnetic Selection. Anal. Chem. 2009; 81:5490–5495. [PubMed: 19480397]

45. Ahmad KM, Oh SS, Kim S, McClellen FM, Xiao Y, Soh HT. Probing the Limits of Aptamer Affinity with a Microfluidic SELEX Platform. PLoS One. 2011; 6:e27051. [PubMed: 22110600]

46. Baaske P, Wienken CJ, Reineck P, Duhr S, Braun D. Optical Thermophoresis for Quantifying the Buffer Dependence of Aptamer Binding. Angew. Chem. Int. Edit. 2010; 49:2238–2241.

47. Heid CA, Stevens J, Livak KJ, Williams PM. Real Time Quantitative PCR. Genome Res. 1996; 6:986–994. [PubMed: 8908518]

48. Stoltenburg R, Reinemann C, Strehlitz B. FluMag-SELEX as an Advantageous Method for DNA Aptamer Selection. Anal. Bioanal. Chem. 2005; 383:83–91. [PubMed: 16052344]

49. Bing T, Yang XJ, Mei HC, Cao ZH, Shangguan DH. Conservative Secondary Structure Motif of Streptavidin-Binding Aptamers Generated by Different Laboratories. Bioorgan. Med. Chem. 2010; 18:1798–1805.

50. Oh SS, Ahmad KM, Cho M, Kim S, Xiao Y, Soh HT. Improving Aptamer Selection Efficiency through Volume Dilution, Magnetic Concentration, and Continuous Washing in Microfluidic Channels. Anal. Chem. 2011; 83:6883–6889. [PubMed: 21774453]

51. Huizenga DE, Szostak JW. A DNA Aptamer That Binds Adenosine and ATP. Biochemistry. 1995; 34:656–665. [PubMed: 7819261]

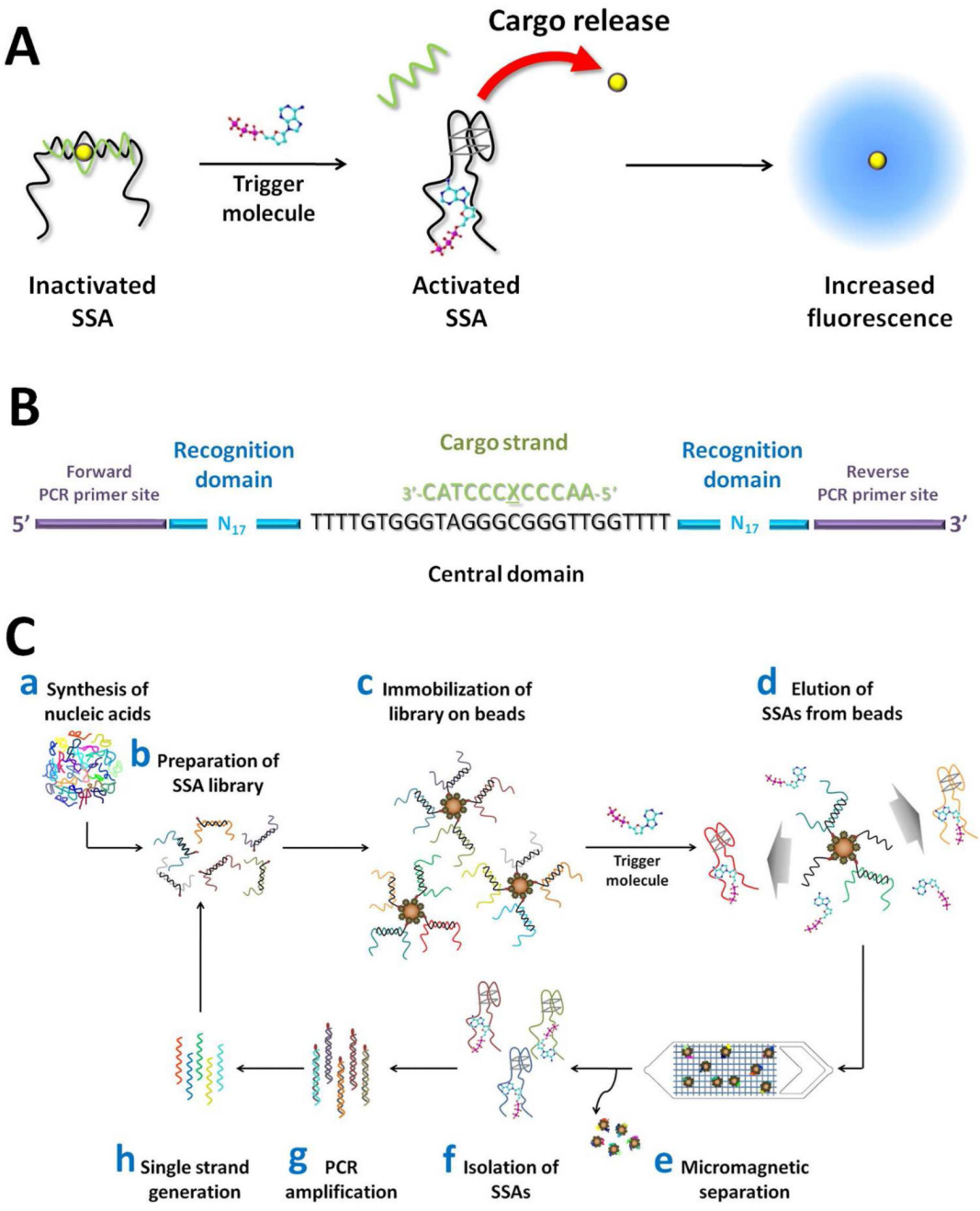

Figure 1.

Design and selection of ATP-specific SSAs. (A) Our SSA was designed to undergo binding-induced structure-switching in response to ATP binding, leading to the release of a cargo strand (green) from its duplex structure. This liberates a pre-loaded ATMND molecule (yellow) from the SSA into solution, unquenching its fluorescence and yielding a detectable signal. (B) We *in vitro* selected our SSA from a library of DNA molecules featuring a 26-base central domain (black) between a pair of randomized 17-base recognition domain sequences (blue), flanked by two 20-base PCR primer sites (purple). The central domain hybridizes to a 12-base cargo strand with an abasic site (green, 'X' denotes the abasic site) that forms a binding pocket for the ATMND cargo. (C) Overview of the selection process.

We synthesized an SSA library containing 100 picomoles of machine-mixed oligonucleotides (a), which we then hybridized with primer site-blocking strands and biotinylated cargo strands (b), allowing us to immobilize the library onto SA-coated magnetic beads (c). We challenged the SSA-bead assemblies with ATP and eluted SSA molecules capable of structure-switching (d), using micromagnetic separation to efficiently retain bead-bound DNAs within a microfluidic chip (e). The isolated SSA pool (f) was then subjected to PCR amplification with biotinylated reverse primers (g), after which we generated and purified single-stranded DNAs from the double-stranded PCR amplicons (h). The resulting enriched SSAs were then prepared for a further round of selection.

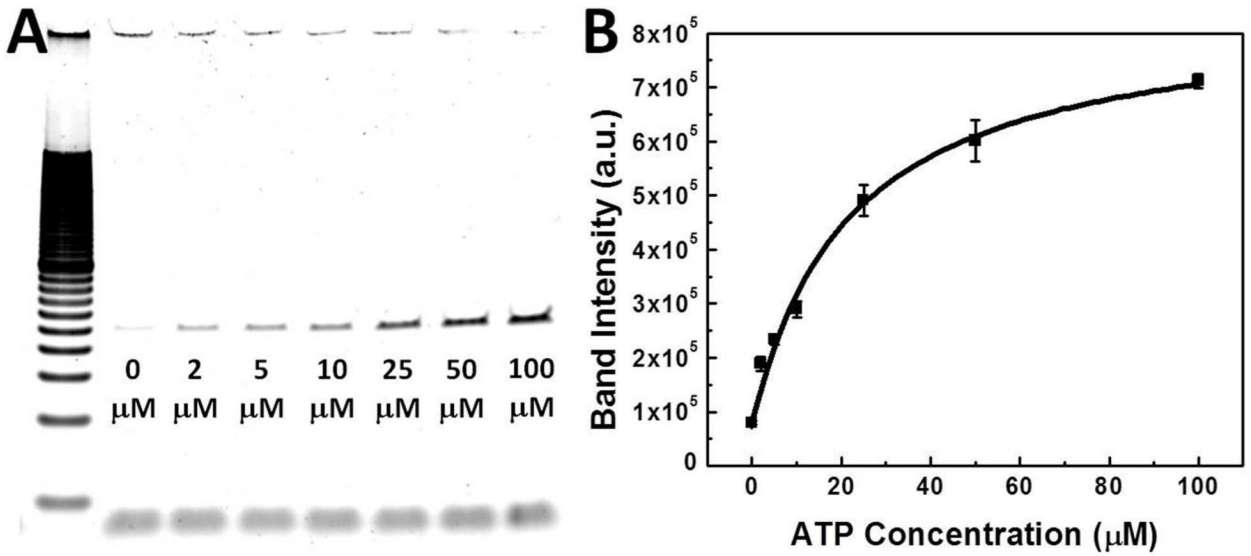

Figure 2.

The R10 pool undergoes structure-switching in an ATP concentration-dependent manner. (A) Gel images of PCR-amplified R10 DNA eluted by ATP concentrations ranging from 2–100 μM (lane 3-8). Lane 1 is 20 bp ladder, lane 2 is buffer only. (B) The half-maximal effective concentration (EC_{50}) of the R10 SSA pool, calculated from the intensity of the sample bands, is 22.1 ± 3.5 μM at a 30 nM concentration of SSA pool/cargo strand (1:1.5 ratio).

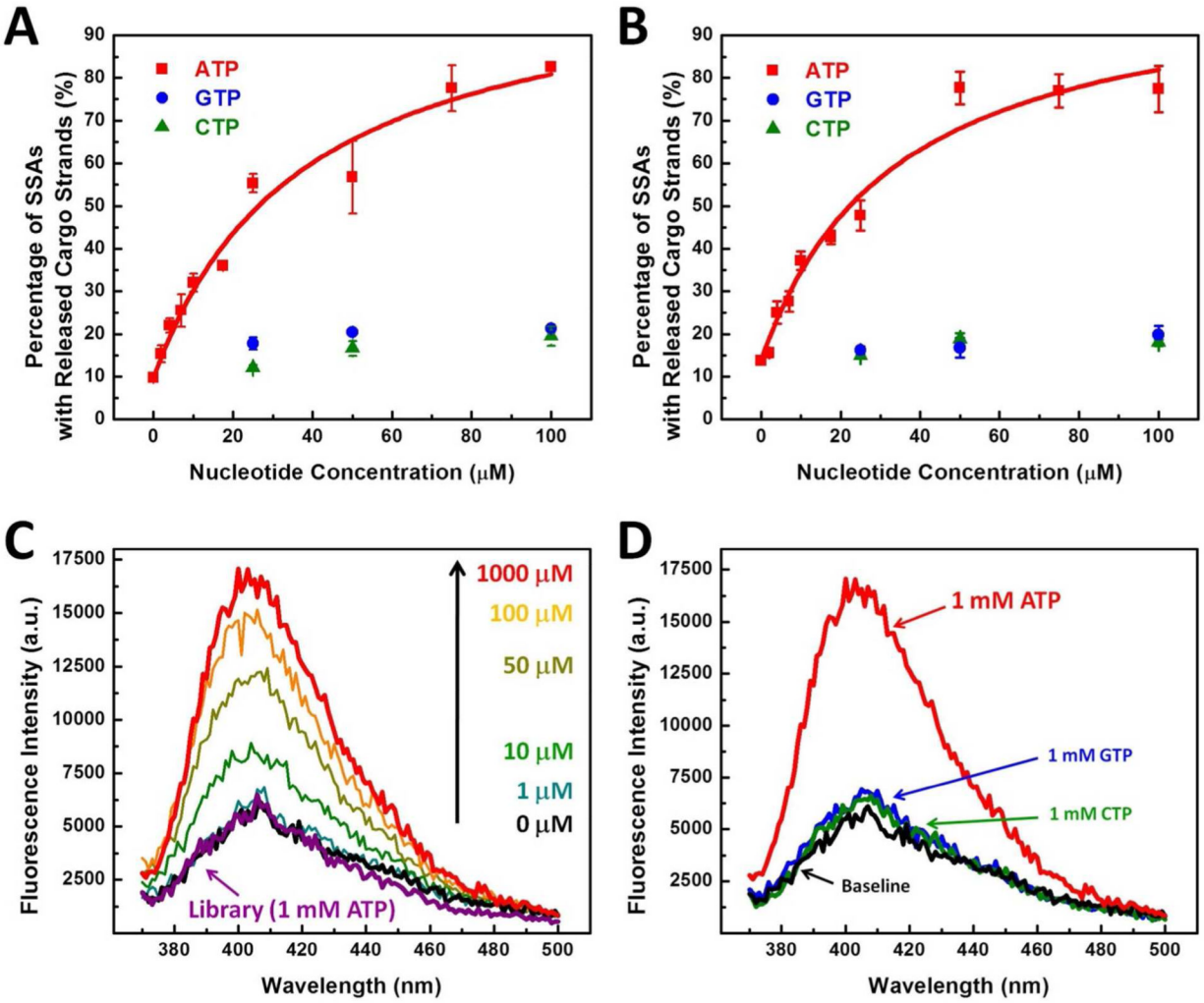

Figure 3.

Sensitivity and target specificity of SSA molecules. RT-PCR measurement of SSA-1 (A) and SSA-2 (B) release from magnetic beads in response to different concentrations of ATP or closely related non-trigger molecules. Both SSAs showed a strong structure-switching response to ATP (red), yielding EC_{50} values of 37.6 ± 8.8 μM and 33.7 ± 7.8 μM for SSA-1 and SSA-2, respectively, at a 30 nM concentration of SSA/cargo strand (1:1.5 ratio). This response was highly specific to ATP, and the fraction of SSAs released by GTP (blue) or CTP (green) was negligible. (C) In the absence of ATP, the ATMND cargo remains sequestered within the abasic site of SSA-1 and emits weak fluorescence signal due to quenching within the duplex structure (black). As the ATP concentration increases, the intensity of fluorescence monotonically increases, with 1 mM ATP yielding a ~170% increase in fluorescence (red) compared to the ATP-free control. In contrast, the response of the unselected random library treated with 1 mM ATP (purple) is indistinguishable from the negative control. (D) SSA-1 emits a strong fluorescent signal in response to 1 mM ATP (red), while GTP (blue) and CTP (green) yield only a negligible increase.

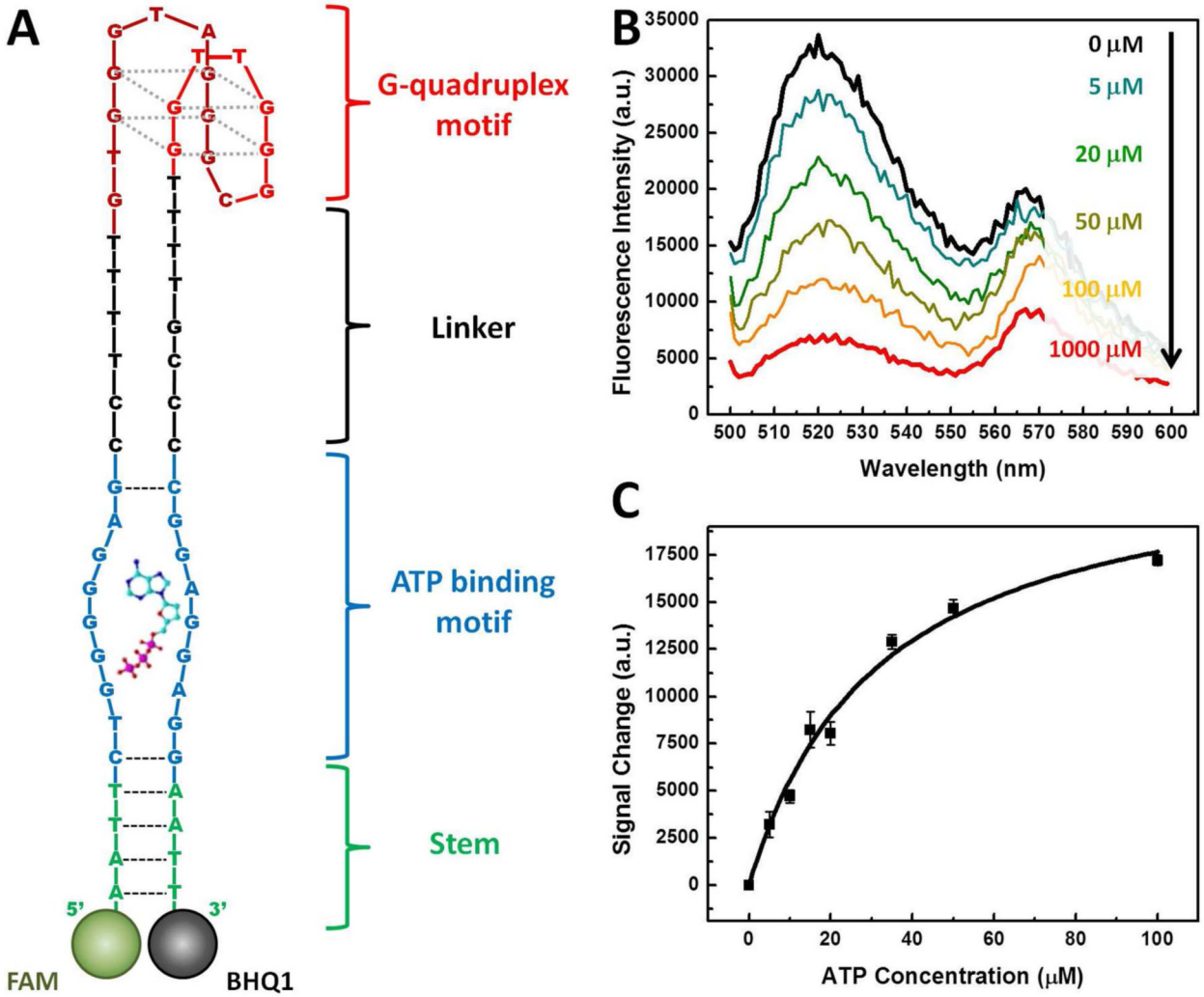

Figure 4.

Characterization of ATP-induced conformational change in SSA-1. (A) The expected structure of SSA-1 after the release of the cargo strand. The structure consists of four domains; the G-quadruplex motif (red) is connected through an unhybridized linker (black) to an ATP binding motif (blue), which is in turn adjacent to a short stem. To confirm that the structure undergoes a shape change upon ATP binding, we labeled the 5′ end with a fluorophore (FAM) and the 3′ end with a quencher (BHQ1). (B) SSA-1 emits strong fluorescence in the absence of ATP. As ATP concentration increases, the fluorescence signal decreases as the conformational change of SSA-1 brings the quencher into close proximity with the fluorophore. (C) Measurements of ATP concentration-dependent signal decrease yield an EC_{50} of 31.8 ± 4.8 μM at a 30 nM concentration of SSA-1/cargo strand (1:1.5 ratio).

Table 1

Dominant SSA consensus sequences from the R10 pool.

Aptamer ID	Percentage of population	SSA sequences without primer sites (5′ → 3′)
SSA-1	**38%**	TTAATTCTGGGGGAGCC-TTTTGTGGGTAGGGCGGGTTGGTTTT-GCCCCGGAGGAGGAATT
SSA-2	**58%**	AGGCTCGTCAACTCGGC-TTTTGTGGGTAGGGCGGGTTGGTTTC-CGGCTTGAAGGAGACGA